Eco-Friendly Synthesis and Biomedical Potential of Zinc Oxide Nanoparticles Using Mentha piperita Aqueous Extract: Comparative Analysis with Chemically Synthesized and Commercial Nanoparticles

Roberta dos Reis, Leonardo da Silva, Joana Pieretti, Benjamin Creusot, Sephora Lahouari, Gregory Francius, Ricardo da Silva, Igor Clarot, Ariane Boudier, Amedea Seabra

Eco-Friendly Synthesis and Biomedical Potential of Zinc Oxide Nanoparticles Using *Mentha piperita* Aqueous Extract: Comparative Analysis with Chemically Synthesized and Commercial Nanoparticles

Roberta A. dos Reis[1,2], Leonardo L. da Silva[1], Joana C. Pieretti[1], Benjamin Creusot[2], Sephora Lahouari[1,2], Gregory Francius[3], Ricardo A. G. da Silva[5], Igor Clarot[2], Ariane Boudier[2,4], Amedea B. Seabra[1*]

[1]Federal University of ABC (UFABC), Santo André, SP, Brazil
[2]Université de Lorraine, CNRS, LRGP, Nancy, France
[3] Université de Lorraine, CNRS, LCPME, Nancy, France
[4]Institut Universitaire de France (IUF), Nancy, France
[5]Federal University of São Paulo (UNIFESP), Diadema, SP, Brazil
* Corresponding author: Amedea Barozzi Seabra
Center for Natural and Human Sciences (CCNH), Federal University of ABC (UFABC), Av. dos Estados 5001, Santo Andre, SP, CEP 09210-580, Brazil, amedea.seabra@ufabc.edu.br

Abstract

Phytosynthesis of zinc oxide nanoparticles (ZnO NPs) using *Mentha piperita* extract offers a sustainable alternative for biomedical applications. This study investigates the synthesis, characterization, and biological properties of biosynthesized ZnO (ZnO Bio NPs) compared to chemically synthesized (ZnO Chem NPs) and commercial ZnO (ZnO Commercial NPs). We explored how peppermint's phytochemicals influence ZnO NP synthesis and biological interactions. Peppermint-derived phytochemicals act as reducing and stabilizing agents while providing antioxidant and anticarcinogenic benefits, potentially enhancing ZnO Bio NPs' therapeutic effects. Our findings reveal that ZnO Bio NPs exhibit superior stability and bioactivity due to plant-based capping agents. ZnO Bio NPs inhibited 52% of DPPH radicals at 15.63 µg/mL, outperforming ZnO Chem and Commercial NPs. In hemocompatibility studies, ZnO Bio NPs showed minimal hemolysis, both with and without protein corona (albumin and fibrinogen), ensuring safer blood interactions. Cytotoxicity assays demonstrated that ZnO Bio NPs had an IC50 of 49.91 µg/mL in human fibroblasts, 3-fold less cytotoxic than ZnO Commercial NPs. These results highlight the potential of peppermint-extract-based ZnO NPs for biomedical applications, offering lower cytotoxicity and greater biocompatibility while providing an eco-friendly alternative to conventional synthesis methods.

Keywords: Biogenic synthesis, Cytotoxicity, Hemocompatibility, Eco-friendly nanoparticle, In vitro analysis.

Introduction

Currently, chemical and physical methods remain the primary approaches for large-scale nanomaterial synthesis. However, these techniques are often associated with environmental hazards, health concerns, high energy consumption, and elevated costs. In contrast, green synthesis offers a sustainable and eco-friendly alternative for producing nanoparticles with distinct properties[1]. This method utilizes natural reagents such as plant extracts, microorganisms, and agricultural by-products, replacing toxic chemicals and significantly reducing the carbon footprint of the synthesis process. Unlike conventional techniques, which generate hazardous waste and pose health risks, green synthesis minimizes environmental pollution while enhancing safety for both ecosystems and human health. Nanoparticles synthesized through this approach exhibit superior biocompatibility, improving their potential for biomedical applications [1–4].

Among plant-mediated nanoparticle synthesis candidates, zinc oxide nanoparticles (ZnO NPs) stand out due to their unique properties [5]. ZnO NPs exhibit distinct physical, chemical, and biological characteristics that differentiate them from bulk zinc oxide. Their versatility in optical, electrical, and magnetic properties makes them suitable for a wide range of applications, including catalysis, energy storage, and biomedical uses [5,6]. However, conventional ZnO NP synthesis often relies on high-temperature processes and hazardous chemicals, which can introduce toxic by-products and reduce biocompatibility [6–8].

Phytosynthesis presents a safer and more sustainable alternative to conventional ZnO NP synthesis, which depends on high energy consumption and chemical reagents that compromise biocompatibility. The phytochemicals in plant extracts not only reduce and stabilize ZnO NPs but also enhance their biocompatibility, making them particularly suitable for drug delivery and regenerative medicine applications [9–12]. Recent studies have demonstrated that biosynthesized ZnO nanoparticles exhibit selective cytotoxicity, effectively targeting cancer cell lines while preserving healthy cells. This selectivity may be attributed to the interaction between ZnO NPs and bioactive compounds in plant extracts, which influence oxidative stress pathways in cancer cells [5,11–13].

Among plant-based reducing agents, *Mentha piperita* (peppermint) stands out due to its rich phytochemical composition, which plays a crucial role in enhancing nanoparticle stability and biocompatibility [10]. Studies have investigated its anti-inflammatory, antimicrobial, and anticancer properties, as well as the effects of hesperidin in cardiovascular protection [14–16] Additionally, *Mentha piperita* is widely available, water-soluble, and rich

in polyphenols and flavonoids, making it an optimal candidate for sustainable nanomaterial synthesis [9,10,17]. The combination of ZnO NPs and *Mentha piperita* extract presents an innovative and eco-friendly approach to bionanotechnology and material science. Lin Loh *et al*. recently synthesized ZnO NPs using agricultural waste from peppermint tea dregs extract, focusing on photocatalytic performance but not evaluating their antioxidant activity, cytotoxicity, or biocompatibility [18].

In light of green chemistry, this study focused on the biogenic synthesis of ZnO NPs using *Mentha piperita* extract (ZnO Bio NPs). *Mentha piperita* was selected due to its exceptional phytochemical profile, particularly its high levels of polyphenols and flavonoids, which enhance nanoparticle stability and biocompatibility. Compared to other plant-based reducing agents, its aqueous extract offers superior solubility, making it more effective in the green synthesis of ZnO NPs. Furthermore, its well-documented medicinal applications, including anti-inflammatory, antimicrobial, and antioxidant properties, reinforce its suitability for sustainable nanomaterial synthesis [10,14,16,19–23]. For comparison, we also synthesized ZnO NPs via a conventional chemical route (ZnO Chem NPs). These nanoparticles were extensively characterized using various techniques to evaluate their physical, chemical, and biological properties. We hypothesized that ZnO Bio NPs synthesized using *Mentha piperita* extract would exhibit superior antioxidant activity and biocompatibility compared to ZnO Chem NPs and ZnO Commercial NPs, owing to the presence of bioactive phytochemicals from the extract

To the best of our knowledge, this is the first report comparing the cytotoxicity of ZnO Bio NPs synthesized with *Mentha piperita* aqueous extract against ZnO Chem NPs and ZnO NPs from Sigma Aldrich (ZnO Commercial NPs) in fibroblast cells. Additionally, this study evaluates hemocompatibility, providing valuable insights into the potential advantages of green synthesis methods using peppermint extract. These findings contribute to the development of biocompatible ZnO NPs with enhanced therapeutic potential for nanomedicine applications.

Materials and Methods

General Reagents

Zinc acetate dihydrate ($Zn(CH_3COO)_2.2\ H_2O$), phosphate-buffered saline tablet (PBS), 4-(2-Hydroxyethyl)piperazine-1-ethanesulfonic acid, *N*-(2-Hydroxyethyl)piperazine-*N*′-(2-ethanesulfonic acid) (HEPES), fetal bovine serum (FBS), Roswell Park Memorial Institute 1640 medium (RPMI 1640), Albumin from human serum (HSA), Fibrinogen from human plasma, MTT reagent [3-(4,5-dimethylthiazol-2-yl)-2,5-diphenyltetrazolium bromide], dimethyl sulfoxide (DMSO), DPPH reagent (2,2-diphenyl-1-picrylhydrazyl), nitric acid (HNO_3), and zinc oxide nanoparticle <100 nm (ZnO Commercial NPs) were obtained from Sigma-Aldrich, MO, USA. Sodium hydroxide (NaOH) was obtained from Synth, Diadema, SP, Brazil. Peppermint (*Mentha piperita*) was acquired from Emporium O Cerealista, São Caetano do Sul, SP, Brazil. All experiments were conducted using analytical grade water purified by reverse osmosis using the Elga DV25 purifier, Ontario, CA.

Characterization of *M. piperita* dried leaves and extract

Fourier-transform infrared spectroscopy (FTIR) was employed to identify functional groups in the peppermint dried leaves, operating at a resolution of 4 cm^{-1} and scanning from 700 cm^{-1} to 4000 cm^{-1} by using an Agilent Cary 630 spectrometer. Thermogravimetric analysis was performed for dried leaves using a TA Instruments Q500 thermogravimetric analyzer. The antioxidant activity of the *M. piperita* extract was measured by DPPH protocol. In brief, 50 mg of dried leaves was suspended in ultrapure water. Subsequently, a serial dilution was performed in ethanol and mixed with 500 µL of a 0.1 mol L^{-1} DPPH solution, and the reaction was kept in the dark for 30 minutes. The reduction in absorbance was measured at 517 nm [24].The DPPH scavenging capacity was calculated using Equation 1:

$$Inhibition\ (\%) = \left(\frac{A0 - A1}{A0}\right) * 100 \qquad \text{Equation 1}$$

Where A_0 and A_1 correspond to the absorbance at 517 nm of the DPPH radical in the absence and presence of the antioxidant agent, respectively.

Phytosynthesis of ZnO NPs (ZnO Bio NPs)

The synthesis of ZnO Bio NPs was accomplished via a biogenic approach using mint extract (*Mentha piperita*) as a reducing agent [25]. Briefly, 2.5 g of peppermint was added into 100 mL of water heated to 75°C. The mixture was stirred at that temperature for 30 min. After agitation, the extract was centrifuged at 4400 rpm for 10 min, and the resulting supernatant was collected and stored. Subsequently, a solution of zinc acetate dihydrate at 0.050 mol. L^{-1} was prepared (50 mL) and mixed with the previously obtained mint extract. The pH of the mixture was adjusted to 9 using a 0.5 mol.L^{-1} NaOH solution and the mixture were stirred for 1 h at 90 °C. The precipitated ZnO Bio NPs were separated by centrifugation, washed thrice with water, frozen, and finally lyophilized [25].

Chemical synthesis of ZnO NPs (ZnO Chem NPs)

The chemical synthesis of ZnO NPs was performed as previously described with some modifications [26]. Briefly, 1 mL of $ZnSO_4.7\ H_2O$ (1 mol. L^{-1}) was added into 13 mL of deionized water. The resulting mixture was heated to 60 °C. Subsequently, 6 mL of NaOH (1 mol. L^{-1}) was added dropwise over 3 minutes into the mixture. The reaction was carried out for 2 h, maintaining the internal reaction temperature within the range of 60-80°C. The resulting white precipitate of ZnOChem NPs was separated, washed, and dried at 60°C under reduced pressure [26].

Characterization of ZnO Bio NPs and ZnO Chem NPs

The characterization of ZnO NPs involved several techniques to assess their physical and chemical properties. The average hydrodynamic size, polydispersity index (PDI) and zeta potential of ZnO NPs were analyzed using a Zetasizer Nano ZS (Malvern Instruments Co). Measurements were performed in aqueous media at 25°C, using a disposable folded capillary zeta cell at a fixed angle of 173°. For X-ray diffraction (XRD) analysis, powder samples were calcined at 750°C for 2 h before data collection. The data were recorded using a Bruker D8 diffractometer with Cu Kα1,2-radiation and analyzed with the Rietveld Method to determine crystallite size and crystallinity index. Fourier-transform infrared spectroscopy (FTIR) was employed with an Agilent Cary 630 spectrometer to identify functional groups on the surface of biogenic ZnO NPs and the extract, operating at a resolution of 4 cm^{-1} and scanning from 700 cm^{-1} to 4000 cm^{-1}. Thermogravimetric analysis (TGA) was conducted using a TA

Instruments Q500 thermogravimetric analyzer to determine organic and inorganic content in ZnO Bio Chem and inorganic part for ZnO Chem NPs. High-resolution transmission electron microscopy (HRTEM) images were acquired using a Carl Zeiss LIBRA® 120 transmission electron microscope and a JEOL 2010 HR-TEM. Samples were dispersed in isopropanol, treated with an ultrasonic bath, and placed on carbon grids for imaging. Atomic force microscopy (AFM) experiments were conducted using the Bruker Bioscope Resolve device at room temperature to analyze the surface morphology and mechanical properties of the nanoparticles. AFM measurements were carried out with a Bioscope Resolve equipment (Bruker AXS, Palaiseau, France) using silicon nitride cantilevers of conical shape (Peakforce HIRS-SSB, Bruker AXS, Palaiseau, France) with spring constants of 0.12 nN/nm. Morphology and peakforce capture images were recorded in PBS at pH 7.4 and room temperature using Peakforce tappingTM mode with scan rate of 1 Hz and 256 force curves per line. Mechanical properties of surface morphology of the nanoparticles were calculated from the analysis of these images. Inductively coupled plasma optical emission spectroscopy (ICP-OES, iCAP PRO, Thermo Scientific) was used for the quantification of zinc content in the ZnO NPs. Briefly, 100 µL of NP suspension were first mineralized with 3.5 mL of ultra-pure water and 2.5 mL of nitric acid 65 %. The samples were then digested using a Microwave Digestion System (Multiwave GO, Anton Paar) for 50 min at 210 °C. The volume was finally adjusted to 10.0 mL with 1 % nitric acid aqueous solution. For zinc quantification, standard solutions of zinc acetate were used to obtain a calibration curve of zinc from 0.1 to 10.0 $mg.L^{-1}$ in 1 % nitric acid (Figure S1). All samples were injected using a peristaltic pump (set at 45 rpm) in the ICP system with argon as auxiliary gas. The nebulizing pressure was 2.1 bar, and the flow rates of the nebulizer and cooler were 0.5 $L.min^{-1}$ and 12.5 $L.min^{-1}$, respectively. Data acquisition was achieved using Qtera software at the working wavelength of 213.856 nm. The antioxidant activities of ZnO Bio NPs, ZnO Chem NPs, and ZnO Commercial NPs were determined using free radical scavenging assay. The DPPH scavenging capacity of each nanoparticle was calculated to quantify the inhibition percentage using the same methodology for the extract. The reduction in absorbance at 517 nm indicated the antioxidant capacity of each NP.

Hemolysis

A total of 1 mL of defibrinated horse blood (Thermofisher) diluted with 19 mL of NaCl 0.9% was mixed and used as blood stock solution. The negative control (0% hemolysis)

was NaCl 0.9%, whereas the positive control (100% hemolysis) was in ultrapure water. In a 2 mL eppendorf, 0.25 mL of stock solution was incubated separately with 1.25 mL of ZnO Bio NPs, ZnO Chem NPs, or ZnO Com NPs in NaCl 0.9% for 2 h at 37°C. All the samples were centrifuged at 4,400 rpm for 4 min. The free hemoglobin measured at 540 nm using the supernatant[27]. NaCl 0.9% was treated as the blank, and its absorbance was subtracted from each reading. The percentage hemolysis was expressed as the ratio of the absorbance of the samples to that of the positive control (water) [27].

Cell viability assay

The cytotoxicity of ZnO Bio NPs, ZnO Chem NPs, and ZnO Com NPs towards normal human fibroblast cells (FN1) was analyzed with an MTT assay. Both cell types were cultured separately in Roswell Park Memorial Institute 1640 medium (RPMI 1640) supplemented with 10% (v/v) fetal bovine serum (FBS) and 1% penicillin/streptomycin at 37°C in an atmosphere containing 5% (v/v) CO_2. The cells were seeded at a density of 4×10^4 cells per well in a 96-well plate for 24 h. Subsequently, the cells were separately treated with ZnO Bio NPs, ZnO Chem NPs, and ZnO Com NPs, at different concentrations for 24 h. As a positive control, 5% DMSO was used. For negative control, water was used. The cells were washed with PBS, then 50 µL of MTT solution (0.3 mg. mL^{-1}), prepared in the RPMI 1640 without FBS, was added to each well, and plates were incubated for 1 h and 30 min at 37 °C in a humidified atmosphere containing 5% CO_2. Finally, the MTT solution was removed from the wells, and formazan crystals were dissolved in 200 µL of dimethyl sulfoxide (DMSO). The plate was gently shaken at room temperature, and the absorbance was measured at 570 nm using a plate reader (++Asys Expert Plus Micropetal Reader, Biochrom, USA). Cells without treatment were used as a control for 100 % cell viability. Each group included quadruplicate assays to confirm the results. The 50% inhibitory concentration (IC_{50}) was determined using sigmoidal regression [27].

Statistical Analysis

Statistical analyses were conducted using GraphPad Prism 8.0 software. One-way ANOVA followed by Tukey's multiple comparisons test or two-way ANOVA followed by Sidak's post hoc test, as outlined in the Figure legends, were used to determine statistical

significance. A p value of less than 0.05 was considered significant. All data are presented as mean ± SD from a minimum of three replicates.

Results and Discussion

Characterization of *M. piperita* leaf and extract

Acknowledging that phenolic compositions are produced by primary and secondary metabolites in plants, it is widely recognized that various factors like soil types, climate conditions, environmental stress, and biomass can significantly influence the composition of flavonoids in plant extracts. Despite these variations, the primary components typically remain present, albeit in differing concentrations [15,23]. As explored in various studies and considering samples from different global locations, the predominant polyphenolic compounds found in peppermint (dried leaves) predominantly include eriocitrin, luteolin, and derivatives of rosmarinic acid [15,23]. Fecka and Turek noted that peppermint leaves contain substantial amounts of caffeic acid derivatives, with levels reaching up to 30.6 mg/g and an average of 13.1 mg/g. Complementary, eriocitrin accounts for 77% of the total flavonoids and 66% of the overall polyphenolic content in peppermint, based on average values from standard peppermint samples [28]. With a comprehensive background from literature on the complete characterization of peppermint, the evaluation of functional groups, thermogravimetric degradation, and antioxidant activity was performed as a preliminary step for phytosynthesis. [28,29].

The FTIR spectroscopy was employed to recognize the functional groups present in the *M. piperita* dried leaves (**Erreur ! Source du renvoi introuvable.**A). The peaks at 3299 and 2922 cm^{-1} are attributed to the O-H, and C-H stretching, respectively. The peaks at 1583 cm^{-1} and 1496 cm^{-1} are attributed to C = O, while 1420 cm^{-1} is assigned to C-H deformation. Peaks at 1264 cm^{-1} and 1028 cm^{-1} are attributed to C-O stretching [30,31], indicating the presence of functional groups found in phytochemicals.

For TGA, as reported by Carballo and coworkers for complex residual organic materials, the initial temperature range, spanning from 20 to 200°C, is marked by the evaporation of residual moisture, often water. Between 200 and 400°C is attributed to the burning of carbohydrates and the breakdown of less dense lignin structures. The fourth region between 400 and 550°C relates to the breakdown of stable aromatic and polynuclear

compounds with high molecular weights. Beyond 550°C suggests the oxidation of stubborn carbon, alongside the decomposition of both mineral and biogenic salts, including carbonates [32]. In general, organic materials decompose into ash, biogenic salts and volatile molecules. As seen in **Erreur ! Source du renvoi introuvable.**B, the dried leaf analysis showed a complex event at the second step. At first, the 11% of water at 175°C, and a second event with a 63.3% englobing since the breakdown of less dense lignin until ashes and salt; similar results are reported in literature[29].

After confirming the presence of phytochemicals, the antioxidant analysis of the extract was conducted. The presence of functional groups such as hydroxyl, carbonyl, and carboxylic acids contributes significantly to nanoparticle synthesis through a redox mechanism, driven by their powerful antioxidant activity[16] . Corroborating, the reducing power of compounds is directly proportional to the antioxidant activity [33–35]. Using the same extraction condition for the synthesis of ZnO Bio NPs (see Experimental Section), the antioxidant activity of *M. piperita* was assessed by DPPH scavenging assay. This approach induces a reduction in absorbance at 517 nm, indicative of the proton transfer reaction facilitated by the herbal antioxidant with the DPPH free radical. The process is monitored through visible spectroscopy until the absorbance reaches a stable level [36]. Figure 1C illustrates that the antioxidant activity of *M. piperita* is concentration-dependent, with nearly 80% of the free radicals eliminated at a concentration of 3.13 $\mu g.mL^{-1}$, highlighting the efficiency of phytochemicals in biosynthesis [37].

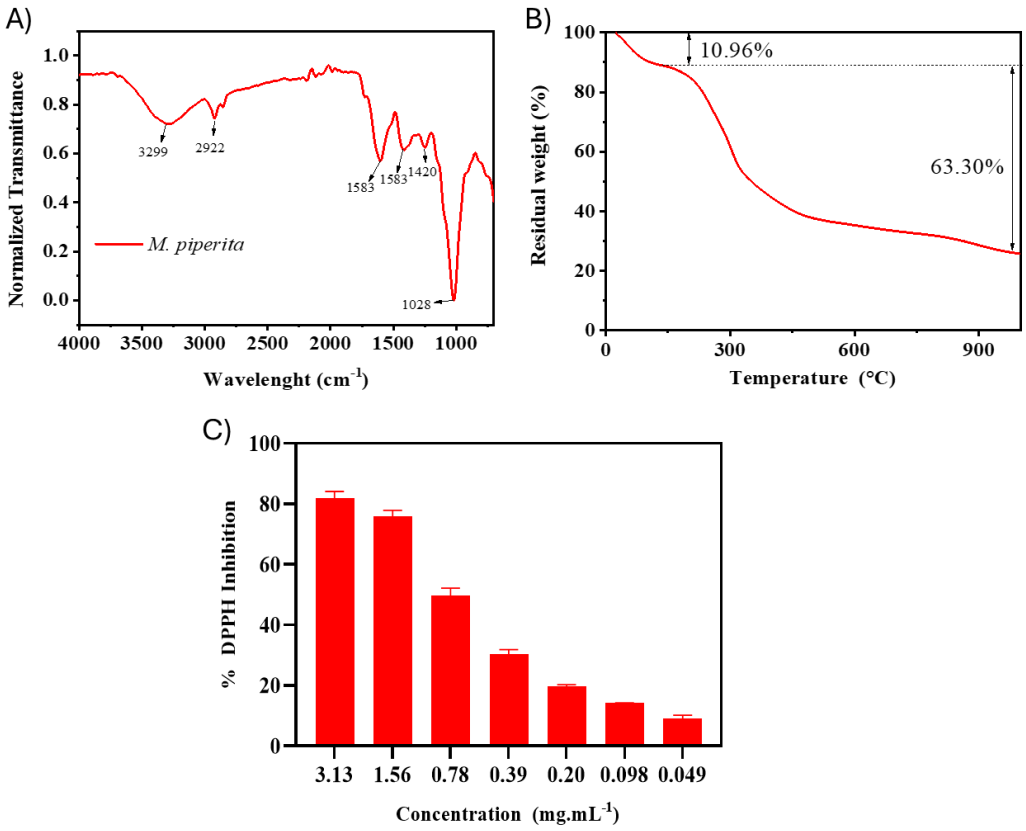

Figure 1. (A) FTIR spectrum of the *M. piperita* leaf (B) TGA analysis of *M. piperita* dried leaf. (C) DPPH radical scavenging activity of *M. piperita* extract.

Synthesis and characterization of ZnO Bio NPs and ZnO Chem NPs

The use of *M. piperita* leaf as source of redox power in NP synthesis is well described in literature, especially for cooper, silver and gold NPs [21,38–40]. Recently, Lin Loh and coworkers [18] developed ZnO NPs from *M. piperita* for photocatalytic performance. Upon introducing the zinc precursor into a homogeneous peppermint extract solution, zinc cations form complexes with functional groups, enhancing stability during nucleation and subsequent NP growth. Consequently, ZnO Bio NPs synthesized in this study demonstrated a distinct brown-yellowish color, suggesting the presence of phytochemicals from the extract. (Figure 2).

For ZnO Chem NPs synthesis, a low-temperature aqueous synthesis method for high-purity ZnO NPs was chosen over the aqueous precipitation synthesis approach [2,26,41]. Only adjusting parameters such as temperature, reaction time, pH of the solution, and the concentration of reagents, it is possible to control the size, shape, and morphology of the ZnO NPs [26,41].

Table 1 shows the average hydrodynamic size, polydispersity index (PDI), and zeta potential (ξ) for ZnO Bio NPs, ZnO Chem NPs and ZnO Commercial NPs. Alike other biogenic NPs, similar results have been reported for PDI, and zeta potential for biogenic synthesis [42,43]. These results indicate that ZnO Bio NPs synthesized with *M. piperita* are in the nanoscale-sized with moderate-to-good dispersion, displaying homogeneous size distribution in aqueous media, and a negative surface charge due to the presence of complex organic groups in ZnO Bio NPs [44] , as found in similar NPs [42,43]. For ZnO Chem NPs, average hydrodynamic size, polydispersity index, and ξ results represented in Table 1, respectively, also agreeing with the literature [41,45–48]. Surprisingly, ZnO Commercial NPs showed a hydrodynamic size, PDI and ξ as similar as ZnO Bio NPs.

Table 1. Hydrodynamic size, zeta potential (ξ) polydispersity index (PDI), crystalline index (CI), crystallite size, zinc percentage (w/w%) of each nanoparticle studied using a concentration of 0.1 mg mL^{-1} in ultrapure water.

Nanoparticle	**Hydrodynamic Size[a] (d. nm)**	**ξ [a] (mV)**	**PDI[a]**	**CI [b]**	**Crystallite size[b] (nm)**	**Zn w/w %**
ZnO Bio NPs	171 ± 5	-18.6 ± 0.2	0.220 ± 0.010	23.1%	19.14 ± 0.83	29.8±0.2[c]
ZnO Chem NPs	105 ± 4	18.6 ± 0.3	0.111 ± 0.020	53.5%	24.31± 6.44	69.9±0.3[c]
ZnO commercial NPs	165 ± 24	-22 ± 0.5	0.285 ± 0.010	nd	nd	79.1 - 81.5 [d]

[a] Dynamic Light Scattering data; Size reported by number and average from mainly peak;

[b] Values estimated using X-ray Diffraction Spectrum of synthesized nanoparticle;

[c] Values estimated using Inductively Coupled Plasma Optical Emission Spectroscopy data (Figure S1and Table S1 in Supporting Information). It involved suspending NPs in water, digestion with HNO_3 and ultrapure water in a microwave-assisted process and measuring the resultant solution using Qtera software for the quantification of zinc content in the ZnO NPs.

[d] According to reported in Sigma Aldrich Product Specification[49].

nd- no data available.

To assess the crystalline structure of ZnO Bio NPs and ZnO Chem NPs, X-ray diffraction was conducted. The results are represented in **Erreur ! Source du renvoi introuvable.**A. The diffraction patterns displaying peaks for the (100), (002), (101), (102), (110), (103), (200), (112), and (201) crystallographic planes at specific peak angles align with the Inorganic Crystal Structure Database ICSD-44477 (ICSD release 2023.2), indicating the formation of ZnO. The XRD data reveals a greater amorphous content in ZnO Bio NPs, compared to ZnO Chem NPs, suggesting the presence of capping derived plant extract on the surface of the NPs. Both ZnO NPs Bio and ZnO NPs Chem display sharp and well-defined peaks. The crystalline index (CI) showed that the amorphous phase is predominant in ZnO Bio NPs, as expected by ash residuals, and the ZnO Chem NPs showed a lower CI value compared to literature [8,50–52]. Gatou and coworkers recently showed the optimized precipitation synthesis in water for this type of nanoparticle [8]. They verified that for this kind of reaction, the zinc sulfate is not indicated, and the calcination after the primary drying is necessary for the obtention of optimal NPs. The Debye-Scherrer formula was applied to calculate the average crystallite size of both NPs based on the three peaks with the highest intensity. The calculated average crystallite size is presented in **Erreur ! Source du renvoi introuvable.**. Contrary to hydrodynamic size measurements, the crystallite size is found to be smaller, which is further elucidated through morphological studies.

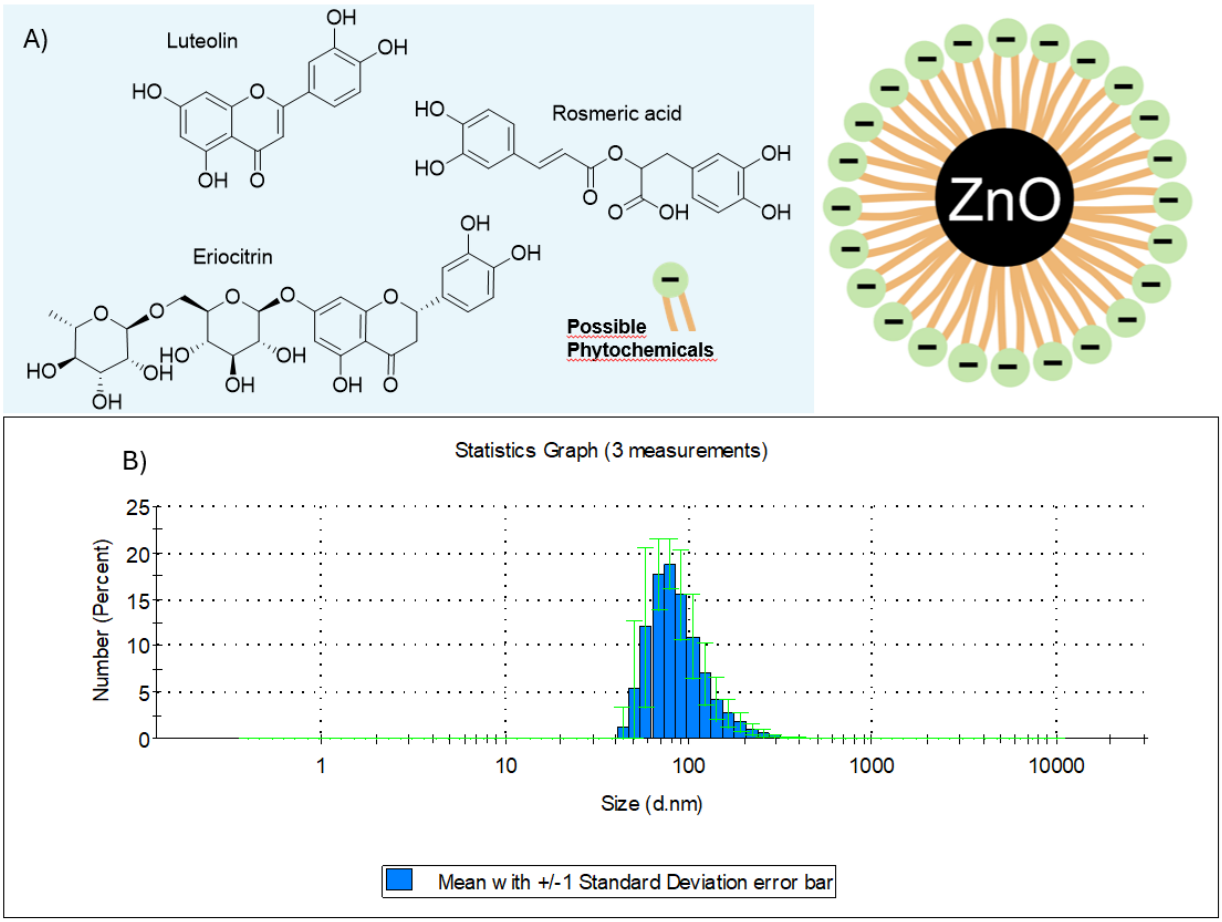

335

336 **Figure 2.** (A) Schematic representation of ZnO Bio NPs synthesized by *M. piperita*
337 extract, showing the main phytochemicals reported in the extract [28]. (B) Hydrodynamic size
338 distribution of ZnO Bio NPs by DLS measurements. For data about ZnO Chem NPs and ZnO
339 Commercial NPs see Supporting Information (Figure S2).

340

341 **Erreur ! Source du renvoi introuvable.**B shows a comparison between the ZnO Bio
342 NPs, ZnO Chem NPs and the dried leaves using FTIR technique to highlight the possible
343 presence of phytochemicals in ZnO Bio NPs. The observed peaks in FTIR for ZnO Bio NPs
344 can be attributed to the presence of phytochemicals, such as glycosides, flavonoids,
345 polyphenols, terpenoids, tannins, carbohydrates, and other reducing sugars [28]. These
346 phytochemicals function as possibly capping agents, since the dried leaves had the same
347 fashion. The ZnO Chem NPs presented the same 3299 cm^{-1} and 2922 cm^{-1} peaks attributed to
348 the OH groups on the surface of ZnO.

349 **Erreur ! Source du renvoi introuvable.**C displays the TGA curves obtained for the
350 synthesized NPs and the peppermint dry leaf. For ZnO Chem NPs (**Erreur ! Source du**
351 **renvoi introuvable.**C), the weight loss was minimum, as expected for pristine NPs [53,54].

However, the peppermint related samples showed a complex TGA events. ZnO Bio NPs exhibit three major weight loss ranges. The initial mass loss of 8.5% occurs around 77 °C, attributed to the evaporation of adsorbed water [55]. The second weight loss of 22.5% is found in the range of 455°C and it is attributed to the thermal degradation of phytochemical compounds on the surface of ZnO Bio NPs, such as carbohydrates, stable aromatic and polynuclear compounds with high molecular weights. Between 455° C and 806° C, it is suggested that the weight loss of approximately 30.5 % and residual of 38.7% is due to the thermal degradation carbon, salt and ZnO core part [32]. It can be inferred that the final residual at 1000°C can be correlated with the inorganic portion of ZnO in the NPs, near ICP-OES Zn mass% determination (**Erreur ! Source du renvoi introuvable.**, see Experimental Section). TGA data revealed the presence of 53 % of biogenic components (phytochemicals) on the surface of ZnO Bio NPs, as depicted in **Erreur ! Source du renvoi introuvable.**C, with 8.5% as water portion and 38.5% of inorganic content.

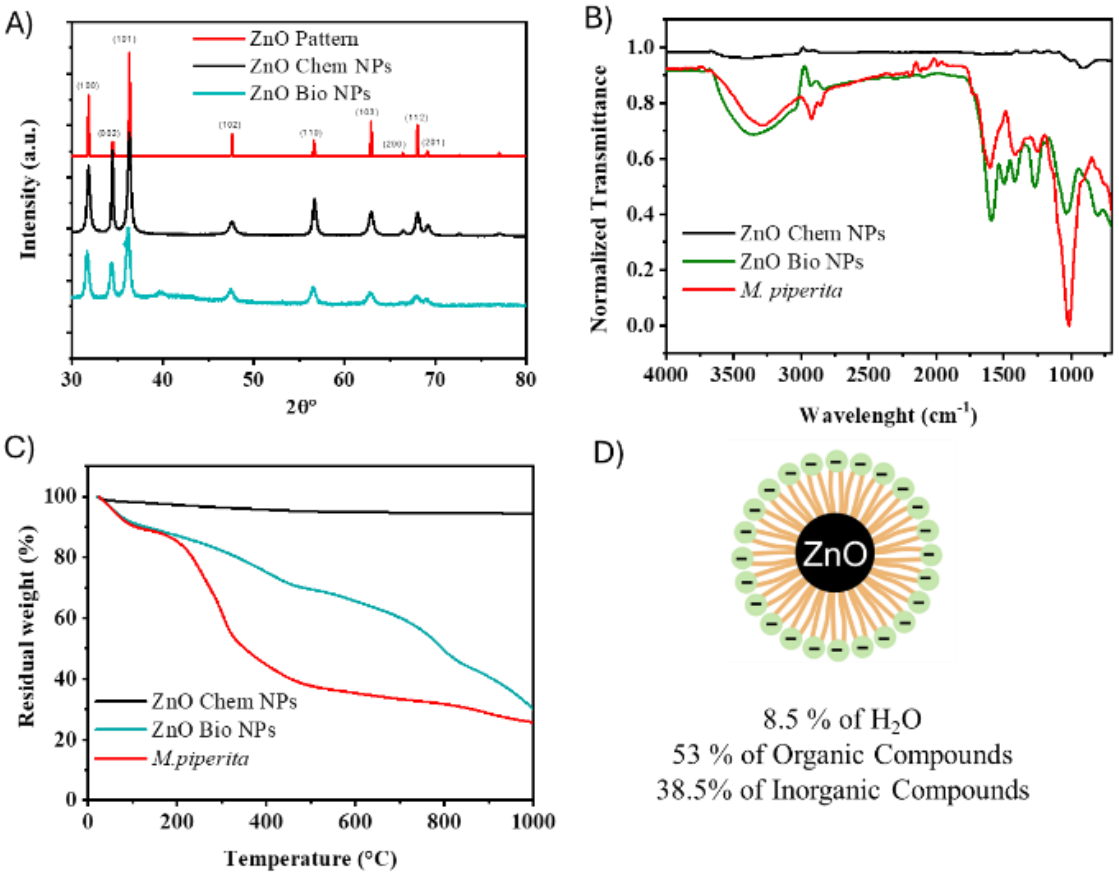

Figure 3. Characterization of ZnO Bio NPs, ZnO Chem NPs. (A) XRD spectra set of ZnO Bio NPs (blue), ZnO Chem NPs (black) and standard ZnO reference from ICSD-44477 (red, ICSD Release 2023.2); (B) FTIR spectra set of the ZnO Bio NPs (blue), ZnO Chem NPs

(black), and *M. piperita* dried leaf (green) (C) TGA analysis of ZnO Bio NPs (blue), ZnO Chem NPs (black), and *M. piperita* dried leaf (green) and zinc acetate dihydrate (grey); (D) Schematic representation of ZnO Bio NPs. For complete analysis, see Supporting Information (Figures S3 to S7).

The morphological analysis, based on HRTEM, showed that ZnO Bio NPs have a petal-like shape as shown in **Erreur ! Source du renvoi introuvable.** A-D. Similarly, ZnO Chem NPs were observed to have petal-like structures, associated with larger sizes, as detailed in **Erreur ! Source du renvoi introuvable.** E-H. These characteristics are consistent with the crystallite size data in **Erreur ! Source du renvoi introuvable.**, which is reflected in the higher standard deviation reported. Pourrahimi *et al*.[41] highlighted that the utilization of diverse zinc salts significantly influences the dimensions of the resulting petal-like structures in water-based synthesis processes, as presented in this work. Specifically, the choice of salt plays a critical role in determining these dimensions. When using zinc sulfate, as precursor in the synthesis, as in ZnO Chem NP, the resulting petal-like sizes are generally larger compared to those produced with zinc acetate (ZnO Bio NPs). This distinction underscores the importance of salt selection in controlling the physical characteristics of the synthesized materials, particularly in terms of their size and morphology [41]. Complementary, the estimated interplanar space was calculated for ZnO Chem NPs with ~0.294 nm, in accordance with the literature [8,56,57]. The ZnO Commercial NPs presented larger petals, as expected from Sigma- Aldrich (Figure S5). The surface morphology for ZnO Bio NPs and ZnO Chem NPs were also analyzed by AFM. For ZnO Chem NPs, the petal shape was confirmed, as presented in HRTEM images. In the 3-dimensional topography map, it was possible to identity the petals stacked forming an agglomerate **Erreur ! Source du renvoi introuvable.**G. Interestingly, the ZnO Bio NPs presented organized structure into 3-dimensional spherical formations, as observed in **Erreur ! Source du renvoi introuvable.**H. For this work, samples were dispersed in isopropyl alcohol for HRTEM, whereas in AFM the sample is prepared in water. Organic solvents could remove the capping, which, therefore, leads to the loss of spherical agglomeration.

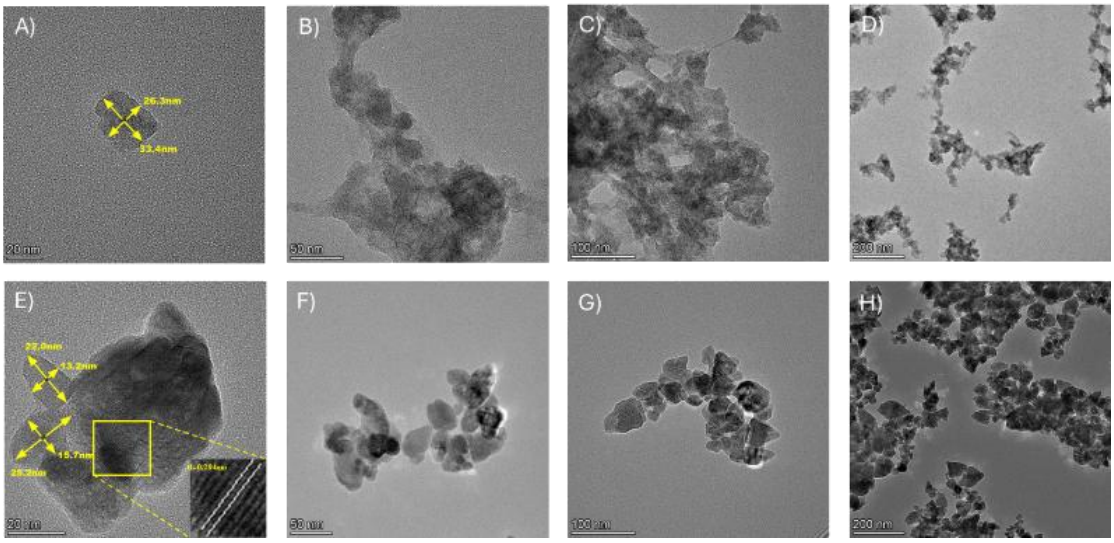

Figure 4. Representative HRTEM images of ZnO Bio NPs (A, B, C, and D) and ZnO Chem NPs (E, F, G, H). Yellow arrows show representative size of petal-like nanoparticles. Yellow square shows the representative Interplanar Spacing (d = 0.294 nm).

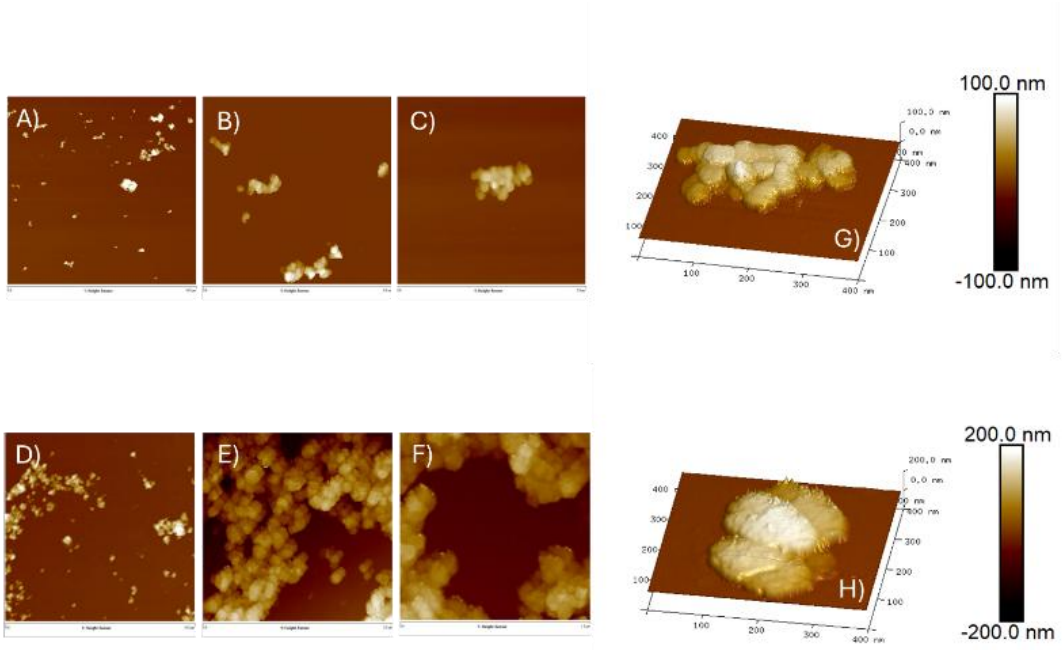

Figure 5. Representative AFM images of ZnO Bio NPs (A, B, C, G) and ZnO Chem NPs (D, E, F and H).

Antioxidant activity of ZnO Bio NPs, ZnO Chem NPs and ZnO Commercial NPs

Figure 6 illustrates the antioxidant activity of all ZnO NPs, expressed as the percentage of DPPH radical scavenging after incubation with different ZnO NP concentrations. The

results reveal a concentration-dependent free radical elimination, with ZnO Bio NPs exhibiting significantly higher antioxidant activity compared to ZnO Chem NPs and ZnO Commercial NPs.

At a concentration of 15.63 $\mu g \cdot mL^{-1}$, ZnO Bio NPs displayed approximately 52% greater antioxidant activity than ZnO Commercial NPs. Additionally, ZnO Bio NPs maintained the highest antioxidant activity across all tested concentrations, supporting the hypothesis that their enhanced radical scavenging ability is primarily due to the incorporation of phytochemicals from *Mentha piperita* extract on their surface. These organic compounds act as capping agents, enhancing stability and bioactivity, which are crucial for biomedical applications.

A comparison with Boppudi *et al*. [58] further highlights the superior antioxidant performance of ZnO Bio NPs. Their study on chemically synthesized ZnO NPs reported approximately 25% inhibition at a higher concentration of 25 $\mu g \cdot mL^{-1}$. In contrast, our ZnO Chem NPs exhibited only 13% inhibition at 15.63 $\mu g \cdot mL^{-1}$, a value similar to that of ZnO Commercial NPs. This suggests that conventional synthesis methods produce ZnO NPs with lower antioxidant efficiency, likely due to the absence of bioactive organic compounds on their surface.. Furthermore, our findings align with Muthuvel *et al*. [59], who demonstrated that biosynthesized ZnO NPs using *Solanum nigrum* extract exhibited a dose-dependent antioxidant response, reaching up to 94% scavenging activity at 500 $\mu g \cdot mL^{-1}$. In contrast, their chemically synthesized ZnO NPs achieved only 60% inhibition at the same concentration. These results further reinforce that biosynthesized ZnO NPs possess superior antioxidant potential compared to chemically synthesized ones, owing to the presence of phytochemicals that enhance free radical scavenging..

The notably high antioxidant activity of ZnO Bio NPs underscores their strong potential for biomedical applications, particularly in therapeutic settings where oxidative stress plays a pivotal role. This enhanced performance is primarily attributed to phytochemicals serving as capping agents, which not only stabilize the nanoparticles but also introduce bioactive functionalities beneficial for medical applications [60].

Given these findings, ZnO Bio NPs emerge as particularly promising candidates for biomedical applications, including neurodegenerative diseases, wound healing, and cancer therapy, where oxidative stress plays a crucial role. Their dual functionality—providing

stability while amplifying therapeutic effects—positions them as superior alternatives to chemically synthesized ZnO NPs in oxidative stress-related treatments.

These results further emphasize the importance of green synthesis approaches, not only for their environmental sustainability but also for their ability to enhance the functional properties of ZnO NPs, making them more effective for biomedical applications than their chemically synthesized counterparts.

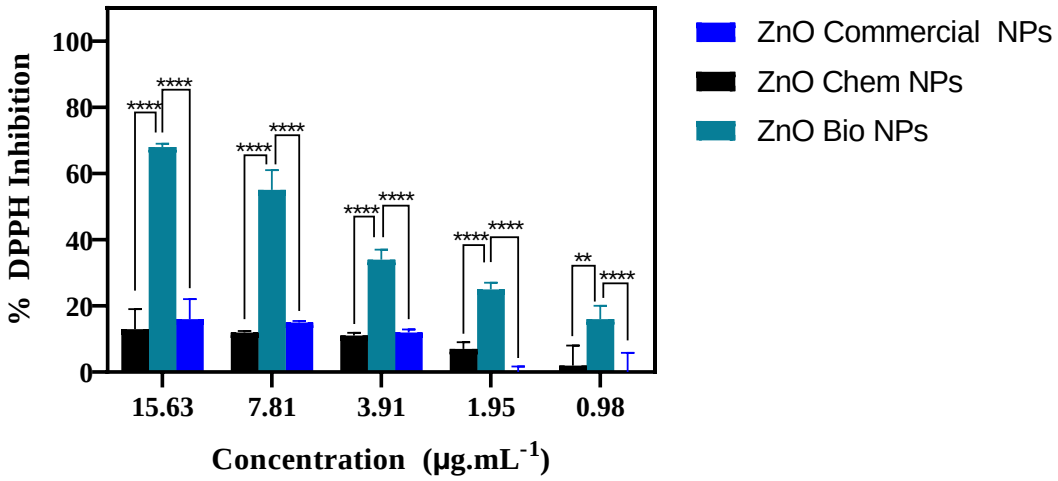

Figure 6. DPPH radical scavenging activity of ZnO Commercial NPs (blue bar), ZnO Chem NPs (black bar), and ZnO Bio NPs (green bar). Asterisks indicate significant statistical differences, where ****p < 0.0001.** p<0.0067, * p<0.0153.

Biocompatibility analysis: hemolysis and cytotoxicity of ZnO Bio NPs, ZnO Chem NPs and ZnO Commercial NPs

The investigation delved into the hemolytic effects of ZnO Commercial NPs, ZnO Bio NPs, and ZnO Chem NPs shedding light on their interaction with plasma proteins and subsequent hemolytic activity. Firstly, the results about hemolysis and cytotoxicity against FN1 are presented in **Erreur ! Source du renvoi introuvable.** and **Erreur ! Source du renvoi introuvable.**. The hemolysis assay results indicate that ZnO Bio NPs exhibited the lowest hemolytic activity (1.5 ± 0.2%), whereas ZnO Commercial NPs (2.4 ± 0.3%) and ZnO Chem NPs (2.3 ± 0.5%) displayed slightly higher hemolytic effects for 10ug/mL. Despite these values being below the general toxicity threshold of 3%, the reduced hemolysis

observed for ZnO Bio NPs suggests improved biocompatibility, likely attributed to the presence of phytochemicals acting as stabilizing and protective agents on the nanoparticle surface. Comparing these findings with existing literature, ZnO NPs synthesized using Gallic acid from *Phyllanthus emblica* demonstrated hemolysis within the 3% toxicity limit, aligning with the biocompatibility observed in ZnO Bio NPs [61]. Additionally, ZnO NPs derived from *Cynara scolymus* leaves showed a remarkably low 0.5% hemolysis at 100 µg/mL, suggesting an even lower impact on red blood cells compared to the current study [62]. Similarly, ZnO NPs synthesized from *Grewia flavescens* also demonstrated excellent hemocompatibility, reinforcing the trend that green-synthesized ZnO NPs tend to induce lower hemolysis than their chemically synthesized counterparts [63]. These comparisons further emphasize the potential of ZnO Bio NPs as a safer alternative for biomedical applications, particularly in drug delivery and intravenous formulations where hemocompatibility is crucial. The presence of bioactive compounds from *Mentha piperita* in ZnO Bio NPs likely contributes to reduced erythrocyte membrane disruption, making them a more biocompatible alternative to conventionally synthesized ZnO NPs.

However, the narrative shifts when considering the impact of NP pre-incubation with proteins, such as albumin or fibrinogen, on hemolysis rates [64]. The discussion regarding the impact of pre-incubation of the NPs with proteins on hemolysis rates gains further complexity when considering the phenomenon known as the protein corona and its potential implications [64]. The formation of the protein corona plays a crucial role in enhancing biocompatibility by forming a protective layer around the NPs, which limits direct interaction between the NP surface and blood cell membranes. This reduces the likelihood of causing cellular damage, especially in the case of ZnO Bio NPs. At the same time, the presence of a protein corona can enhance the interaction between NPs and blood cells, potentially leading to increased hemolysis rates, depending on the type of protein involved [65]. Using 10% of these proteins in human blood real concentration (**Erreur ! Source du renvoi introuvable.**, HSA 3.5 $g.L^{-1}$ [66] and fibrinogen 0.2 $g.L^{-1}$ [67]), the results reveal an increase in hemolysis, particularly with ZnO Chem NPs. At a concentration of 10 $\mu g.mL^{-1}$ of ZnO Chem NPs, hemolysis rates rise to approximately 7%, surpassing the acceptable threshold set by ISO10993-4 standards [68]. While ZnO Bio NPs and ZnO Commercial NPs variants exhibit lower hemolysis rates under the same conditions, they still breach the 5 % mark, albeit to a lesser extent.

According to literature, albumin, the main transport protein in the bloodstream, is essential for transporting various drugs. Albumin is also identified as the major transport

protein for zinc in plasma, binding the majority of plasma zinc and facilitating its systemic distribution [69]. The findings suggest that the protective effect of albumin may result from the high affinity of ZnO NPs for albumin, which forms a corona around the NP, thereby reducing its direct interaction with cellular membranes. Studies have shown that ZnO NPs interact with albumin to form an albumin-ZnO complex, which alters the conformation of albumin and can increase hemolysis due to changes in protein structure and subsequent interactions with cell membranes [70,71]. Nevertheless, for fibrinogen, Mitjans and coworkers showed that despite being present in lower concentrations in plasma compared to albumin, fibrinogen is found in greater amounts on the ZnO NPs, indicating its preferential adsorption [71]. Given the preferential interaction with fibrinogen, the hemolytic effect decreased for all nanoparticles (Table 2), particularly for ZnO Bio NPs, suggesting a unique stabilization effect provided by fibrinogen adsorption, which can potentially mitigate the cytotoxic impacts. This preferential adsorption of fibrinogen to the ZnO Bio NPs, instead of interacting aggressively with blood cell membranes, indicates their superior biocompatibility, making them more suitable for potential clinical applications.

The cytotoxicity assay was performed using the MTT method to evaluate the toxicity of ZnO Commercial NPs, ZnO Bio NPs, and ZnO Chem NPs against FN1 fibroblast cells. Following the hemocompatibility assay, FN1 cells were exposed to increasing concentrations (10 to 100 $\mu g \cdot mL^{-1}$) of ZnO NPs for 24 hours to assess cell viability. As shown in Figure 7 and Table 2, all ZnO NPs exhibited a dose-dependent cytotoxic effect, leading to reduced cell viability as the concentration increased.

Notably, ZnO Bio NPs demonstrated the highest biocompatibility, with an IC_{50} value of 49.91 $\mu g \cdot mL^{-1}$, significantly higher than ZnO Chem NPs (19.81 $\mu g \cdot mL^{-1}$) and ZnO Commercial NPs (16.35 $\mu g \cdot mL^{-1}$). These findings suggest that the phytochemicals present in ZnO Bio NPs confer a protective effect, reducing their cytotoxicity compared to chemically synthesized nanoparticles.

Dinga *et al.* [72] evaluated the cytotoxicity of ZnO NPs synthesized using *Melia azedarach* seed extract against HepG2 cells, further supports the lower toxicity of biosynthesized ZnO NPs. Their study reported an IC_{50} of 27.6 $\mu g \cdot mL^{-1}$ for green-synthesized ZnO NPs, which is intermediate between our ZnO Bio NPs and the ZnO Chem NPs.

For normal cell cytotoxicity, El-Belely *et al* [73] reported an IC50 of 53.34 µg/mL for normal WI38 cells, suggesting a similar cytotoxic effect to normal fibroblasts. This trend

aligns with findings from Maheswaran *et al*. [74], where green-synthesized ZnO NPs using *Musa acuminata* extract exhibited an IC50 of 78.4 µg·mL^{-1} on Vero cells, significantly higher than their chemically synthesized counterparts (IC50 = 31.2 µg·mL^{-1}). Similarly, Shaban *et al*. [75]reported that ZnO NPs synthesized from pomegranate peel extract displayed an IC50 of 240 µg·mL^{-1} further supporting the protective effects of bioactive compounds in green synthesis.

These findings highlight a common trend in biosynthesized ZnO NPs—reduced toxicity toward normal cell. This is likely attributed to the presence of bioactive compounds from *Mentha piperita*, which act as stabilizing and capping agents, mitigating oxidative stress in healthy cells. The superior biocompatibility observed in ZnO Bio NPs suggests their potential for biomedical applications, particularly in areas where reduced cytotoxicity is essential, such as drug delivery, wound healing, and antioxidant therapies.

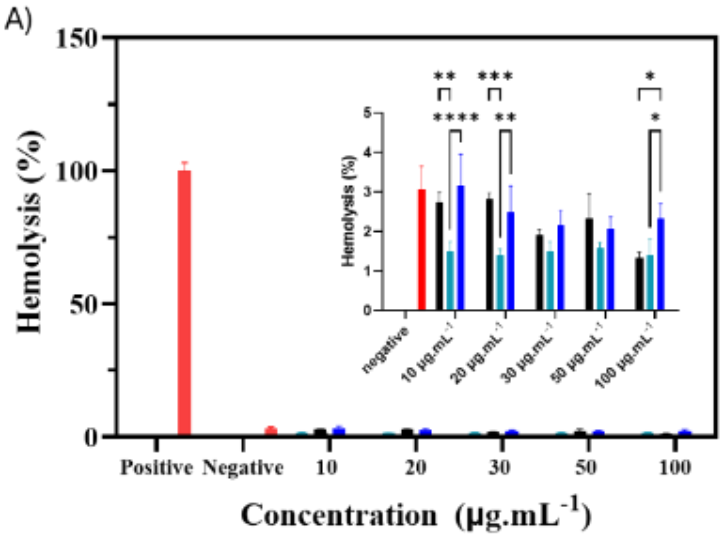

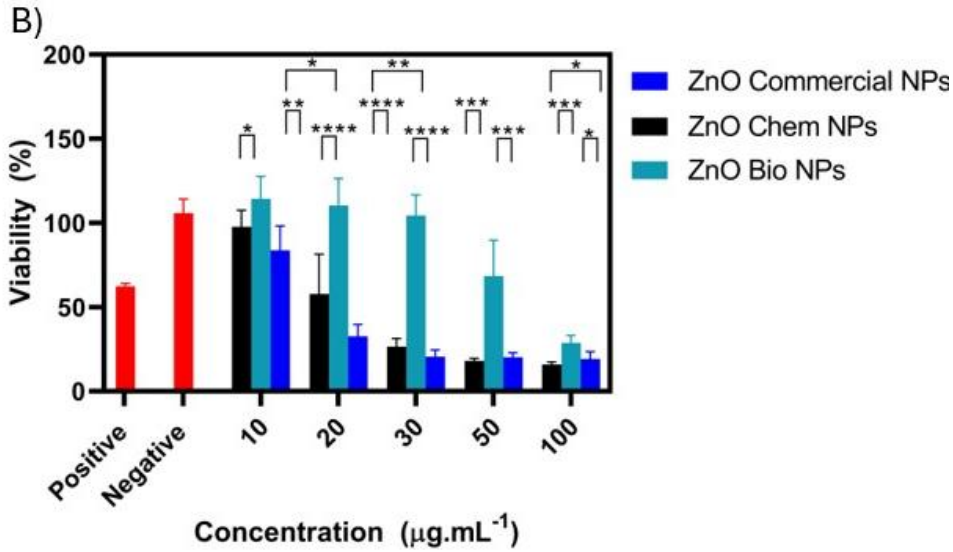

Figure 7. (A) Hemolytic activity of ZnO Commercial NPs (blue bar), ZnO Chem NPs (black bar), ZnO Bio NPs (green bar) at different concentrations at room temperature. Positive control: H_2O. Negative control: 0.9%NaCl. The data is expressed as the mean ± standard deviation of three replicates. ANOVA Two way with Tukey's post hoc test. Asterisks indicate significant statistical differences, where **** $p < 0.0001$.** $p=0.0017$, * $p=0.0174$. (B) Cytotoxicity assay of FN1 cells treated with different nanoparticles at different concentrations; ZnO Commercial NPs (blue bar), ZnO Chem NPs (black bar), and ZnO Bio NPs (green bar). Positive control: 5% DMSO. Negative control: H_2O. The data is expressed as the mean ± standard deviation of ten replicates. ANOVA Two way with Tukey's post hoc test. Asterisks indicate significant statistical differences, where *$p<0.05$, **$p<0.01$***, $p = 0.0001$ and **** $p < 0.0001$.

Table 2. Hemolysis activity of 10 $\mu g.mL^{-1}$ of each NP with and without 1h of pre-incubation at 37°C with Human Serum Albumin (HSA) and fibrinogen. IC_{50} against FN1 cell lines treated with ZnO Commercial, ZnO Chem, and ZnO Bio NPs after 24 h.

	Hemolysis in 0.9% NaCl with Nanoparticle at 10 $\mu g.mL^{-1}$			**Cytotoxicity against FN1**
	Without pre-incubation	HSA 3.5$g.L^{-1}$ pre-incubation	Fibrinogen 0.2$g.L^{-1}$ pre-incubation	IC50 ($\mu g.mL^{-1}$)
ZnO Commercial NPs	2.4± 0.3	7.7±0.8	5.1±0.8	16.35
ZnO Bio NPs	1.5±0.2	5.0±0.8	3.2±0.5	19.81
ZnO Chem NPs	2.3±0.5	6.8±0.6	4.9±1.1	49.91

Conclusions

ZnO NPs were successfully synthesized by phytosynthesis using *M. piperita* extract as reducing and capping agent. Both ZnO Bio NPs and ZnO Chem NPs were characterized by FTIR, DLS, HTEM, XRD, and TGA analysis. FTIR confirmed the presence of organic

compounds from the *M. piperita* extract in the ZnO Bio NPs. The ZnO Bio NPs displayed impressive antioxidant activity, with approximately 52% inhibition of DPPH radicals at a concentration of 15.63 $\mu g.mL^{-1}$, surpassing the performance of commercially available ZnO NPs.

The biological compatibility of the NPs was assessed through hemolysis and cytotoxicity assays. In studies involving the interaction with blood, ZnO Bio NPs displayed minimal hemolytic activity (1.5%) compared to ZnO Chem NPs (2.7%) and ZnO Commercial NPs (3.2%). These results underscore the enhanced hemocompatibility of ZnO Bio NPs, attributed to the presence of phytochemicals that act as a protective layer, reducing interactions with blood cells. Furthermore, in cytotoxicity assays, ZnO Bio NPs exhibited higher IC50 values (49.91 $\mu g.mL^{-1}$), demonstrating less cytotoxicity towards fibroblast cells (FN1) when compared to ZnO Chem NPs and ZnO Commercial NPs. This highlights the potential of ZnO Bio NPs as a safer alternative for biomedical applications.

These findings validate the hypothesis that ZnO Bio NPs synthesized using *M. piperita* extract exhibit superior biocompatibility and antioxidant activity compared to ZnO Chem NPs and ZnO Commercial NPs. The utilization of phytochemicals in peppermint not only enhances the therapeutic efficacy of ZnO NPs but also aligns with green chemistry principles, minimizing environmental impact and contributing to sustainable bionanotechnology. Our findings provide valuable insights into the potential advantages of green synthesis methods using peppermint extract, contributing to the development of biocompatible NPs with enhanced therapeutic potential for applications in nanomedicine.

Acknowledgements. The authors are thankful for the financial support from Coordenação de Aperfeiçoamento de Pessoal de Nível Superior - Brasil (CAPES) (Finance Code 001 (88887.872138/2023-00) (RAR), Finance Code 001 (88881.711920/2022−01) (ABS/AB) and CAPES/COFECUB Campus France program Ph-C983/23, 49445SA). We are also thankful for financial support from CNPq (313117/2019−5 (ABS), and from São Paulo Research Foundation (FAPESP, grants 2022/14645-2 and 2024/12112-2 (ABS), 2023/16363-7 (RAR), 2022/13444-3 (LLS), 2020/03646-2 (JCP)).

Author contributions. Roberta A. dos Reis: methodology, investigation, data curation, writing-original, draft, validation; Leonardo L. da Silva: investigation. Joana C. Pieretti: investigation; Benjamin Creusot: investigation Sephora Lahouari: investigation.

Gregory Francius: investigation and Ricardo A. g. da Silva: investigation. Igor Clarot: writing-review & editing. Ariane Boundier: conceptualization, writing-review & editing. Amedea B. Seabra: conceptualization, writing-review & editing, supervision, funding. All authors have given approval to the final version of the manuscript.

Data availability. The data supporting this article have been included as part of the ESI.

Declarations

Conflict of interest. The authors declare no competing interests.

Ethical approval and consent to participate. Since animals or humans cannot be used in this study, no ethical approval is necessary

References

[1] D. Gupta, A. Boora, A. Thakur, T.K. Gupta, Green and sustainable synthesis of nanomaterials: Recent advancements and limitations, Environ Res 231 (2023) 116316. https://doi.org/10.1016/J.ENVRES.2023.116316.

[2] R. Sreekanth, S. Naveen Kumar, M. Madhusudhan Reddy, P. Pattar, B. V. Damodar Reddy, Investigating the effect of acidic and basic precipitation on the antibacterial activity of ZnO nanoparticles against Gram-negative and Gram-positive bacteria, J Mater Chem B 12 (2024) 2180–2196. https://doi.org/10.1039/D3TB02119J.

[3] R. Hamed, R.Z. Obeid, R. Abu-Huwaij, Plant mediated-green synthesis of zinc oxide nanoparticles: An insight into biomedical applications, Nanotechnol Rev 12 (2023). https://doi.org/10.1515/NTREV-2023-0112/ASSET/GRAPHIC/J_NTREV-2023-0112_FIG_001.JPG.

[4] B. de M. Santana, G.M. Armentano, D.A.S. Ferreira, C.S. de Freitas, M.S. Carneiro-Ramos, A.B. Seabra, M. Christodoulides, In Vitro Bactericidal Activity of Biogenic Copper Oxide Nanoparticles for Neisseria gonorrhoeae with Enhanced Compatibility for Human Cells, ACS Appl Mater Interfaces 16 (2024) 21633–21642. https://doi.org/10.1021/ACSAMI.4C02357/SUPPL_FILE/AM4C02357_SI_001.PDF.

[5] A. Wafi, M.M. Khan, Green synthesized ZnO and ZnO-based composites for wound healing applications, Bioprocess and Biosystems Engineering 2024 (2024) 1–22. https://doi.org/10.1007/S00449-024-03123-Z.

[6] M.L. Popa, M.D. Preda, I.A. Neacșu, A.M. Grumezescu, O. Ginghină, Traditional vs. Microfluidic Synthesis of ZnO Nanoparticles, International Journal of Molecular Sciences 2023, Vol. 24, Page 1875 24 (2023) 1875. https://doi.org/10.3390/IJMS24031875.

[7] T. Thilagavathi, D. Geetha, Low-temperature hydrothermal synthesis and characterization of ZnO nanoparticles, Indian Journal of Physics 87 (2013). https://doi.org/10.1007/s12648-013-0290-8.

[8] M.A. Gatou, K. Kontoliou, E. Volla, K. Karachalios, G. Raptopoulos, P. Paraskevopoulou, N. Lagopati, E.A. Pavlatou, Optimization of ZnO Nanoparticles' Synthesis via Precipitation Method Applying Taguchi Robust Design, Catalysts 2023, Vol. 13, Page 1367 13 (2023) 1367. https://doi.org/10.3390/CATAL13101367.

[9] N. Hudz, L. Kobylinska, K. Pokajewicz, V. Horčinová Sedláčková, R. Fedin, M. Voloshyn, I. Myskiv, J. Brindza, P.P. Wieczorek, J. Lipok, Mentha piperita: Essential Oil and Extracts, Their Biological Activities, and Perspectives on the Development of New Medicinal and Cosmetic Products, Molecules 2023, Vol. 28, Page 7444 28 (2023) 7444. https://doi.org/10.3390/MOLECULES28217444.

[10] S. Akhtar, M. Adnan, S. Sharif, S.A. Khan, Modulation Response of Biologically Synthesized ZnO Nanoparticles Using Mentha piperita L. on the Physio-Chemical Parameters of Pisum sativum L., Journal of Plant Nutrition and Soil Science 188 (2025) 151–164. https://doi.org/10.1002/JPLN.202400268.

[11] X.T. Tran, T.T.L. Bien, T. Van Tran, T.T.T. Nguyen, Biosynthesis of ZnO nanoparticles using aqueous extracts of Eclipta prostrata and Piper longum: characterization and assessment of their antioxidant, antibacterial, and photocatalytic properties, Nanoscale Adv 6 (2024) 4885–4899. https://doi.org/10.1039/D4NA00326H.

[12] M.E. Cervantes-Gaxiola, F.A. Vázquez-González, E.Y. Rios-Iribe, P.F. Méndez-Herrera, C. Leyva, Effect of pH on the green synthesis of ZnO nanoparticles using Sorghum bicolor seed extract and their application in photocatalytic dye degradation, Mater Lett 372 (2024) 136982. https://doi.org/10.1016/J.MATLET.2024.136982.

[13] M.A.A.H. Allah, H.K. Ibrahim, H.A. Alshamsi, Enhanced adsorption, anticancer and antibacterial potentials of Pontederia crassipes L. extract mediated ecofriendly synthesized ZnO/biochar nanohybrid, Inorg Chem Commun 171 (2025) 113538. https://doi.org/10.1016/J.INOCHE.2024.113538.

[14] N. Hudz, L. Kobylinska, K. Pokajewicz, V. Horčinová Sedláčková, R. Fedin, M. Voloshyn, I. Myskiv, J. Brindza, P.P. Wieczorek, J. Lipok, Mentha piperita: Essential Oil and Extracts, Their Biological Activities, and Perspectives on the Development of New Medicinal and Cosmetic Products, Molecules 2023, Vol. 28, Page 7444 28 (2023) 7444. https://doi.org/10.3390/MOLECULES28217444.

[15] K. Kapp, E. Hakala, A. Orav, L. Pohjala, P. Vuorela, T. Püssa, H. Vuorela, A. Raal, Commercial peppermint (Mentha × piperita L.) teas: Antichlamydial effect and polyphenolic composition, Food Research International 53 (2013) 758–766. https://doi.org/10.1016/J.FOODRES.2013.02.015.

[16] R. Singh, M.A.M. Shushni, A. Belkheir, Antibacterial and antioxidant activities of Mentha piperita L., Arabian Journal of Chemistry 8 (2015) 322–328. https://doi.org/10.1016/J.ARABJC.2011.01.019.

[17] M. Saad, H. Tahir, S. Mustafa, O.A. Attala, W.A. El-Saoud, K.A. Attia, W.M. Filfilan, J. Zeb, Polyvinyl Alcohol Assisted Iron–Zinc Nanocomposite for Enhanced Optimized Rapid Removal of Malachite Green Dye, Nanomaterials 2023, Vol. 13, Page 1747 13 (2023) 1747. https://doi.org/10.3390/NANO13111747.

[18] X. Lin Loh, Z. Xian Ooi, Y. Peng Teoh, S. Hoong Shuit, U. Tunku Abdul Rahman, K. Campus, B. Barat, A. Rahman, S. Long Campus, B. Sungai Long, M. Correspondence Zhong Xian Ooi, Synthesis and characterization of zinc oxide nanoparticles using peppermint tea (Mentha piperita) dregs extract and their photocatalytic performance, Environ Prog Sustain Energy 42 (2023) e14202. https://doi.org/10.1002/EP.14202.

[19] A. Eftekhari, A. Khusro, E. Ahmadian, S.M. Dizaj, L. Dinparast, M.B. Bahadori, A. Hasanzadeh, M. Cucchiarini, Phytochemical and nutra-pharmaceutical attributes of Mentha spp.: A comprehensive review, Arabian Journal of Chemistry 14 (2021) 103106. https://doi.org/10.1016/J.ARABJC.2021.103106.

[20] E.A. Luță, A. Biță, A. Moroșan, D.E. Mihaiescu, M. Ghica, D.P. Mihai, O.T. Olaru, T. Deculescu-Ioniță, L.E. Duțu, M.L. Popescu, L. Costea, G.M. Nitulescu, D. Lupuliasa, R. Boscencu, C.E. Gîrd, The Influence of Phytosociological Cultivation and Fertilization on Polyphenolic Content of Menthae and Melissae folium and Evaluation of Antioxidant Properties through In Vitro and In Silico Methods, Plants 11 (2022) 2398. https://doi.org/10.3390/PLANTS11182398/S1.

[21] A. Khatoon, F. Khan, N. Ahmad, S. Shaikh, S.M.D. Rizvi, S. Shakil, M.H. Al-Qahtani, A.M. Abuzenadah, S. Tabrez, A.B.F. Ahmed, A. Alafnan, H. Islam, D. Iqbal, R. Dutta, Silver nanoparticles from leaf extract of Mentha piperita: Eco-friendly synthesis and effect on acetylcholinesterase activity, Life Sci 209 (2018) 430–434. https://doi.org/10.1016/J.LFS.2018.08.046.

[22] Z. Sun, H. Wang, J. Wang, L. Zhou, P. Yang, Chemical Composition and Anti-Inflammatory, Cytotoxic and Antioxidant Activities of Essential Oil from Leaves of Mentha piperita Grown in China, PLoS One 9 (2014) e114767. https://doi.org/10.1371/JOURNAL.PONE.0114767.

[23] S.F. Hendawy, A.G. El Gendy, E.A. Omer, L. Pistelli, L. Pistelli, Growth, Yield and Chemical Composition of Essential Oil of Mentha piperita var. multimentha Grown Under Different Agro-ecological Locations in Egypt, Journal of Essential Oil Bearing Plants 21 (2018) 23–39. https://doi.org/10.1080/0972060X.2017.1423247.

[24] M.T. Pelegrino, M.Y. Kohatsu, A.B. Seabra, L.R. Monteiro, D.G. Gomes, H.C. Oliveira, W.R. Rolim, T.A. de Jesus, B.L. Batista, C.N. Lange, Effects of copper oxide nanoparticles on growth of lettuce (Lactuca sativa L.) seedlings and possible implications of nitric oxide in their antioxidative defense, Environ Monit Assess 192 (2020) 232. https://doi.org/10.1007/s10661-020-8188-3.

[25] S. Narath, S.K. Koroth, S.S. Shankar, B. George, V. Mutta, S. Wacławek, M. Černík, V.V.T. Padil, R.S. Varma, Cinnamomum tamala leaf extract stabilized zinc oxide nanoparticles: A promising photocatalyst for methylene blue degradation, Nanomaterials 11 (2021). https://doi.org/10.3390/nano11061558.

[26] A. Moezzi, M. Cortie, A. McDonagh, Aqueous pathways for the formation of zinc oxide nanoparticles, Dalton Transactions 40 (2011). https://doi.org/10.1039/c0dt01748e.

[27] J.C. Pieretti, M.C. Gonçalves, G. Nakazato, A.C. Santos de Souza, A. Boudier, A.B. Seabra, Multifunctional hybrid nanoplatform based on Fe3O4@Ag NPs for nitric oxide delivery: development, characterization, therapeutic efficacy, and hemocompatibility, J Mater Sci Mater Med 32 (2021). https://doi.org/10.1007/s10856-021-06494-x.

[28] I. Fecka, S. Turek, Determination of water-soluble polyphenolic compounds in commercial herbal teas from Lamiaceae: Peppermint, melissa, and sage, J Agric Food Chem 55 (2007) 10908–10917. https://doi.org/10.1021/JF072284D/ASSET/IMAGES/LARGE/JF-2007-02284D_0005.JPEG.

[29] M. Masłowski, A. Aleksieiev, J. Miedzianowska, K. Strzelec, Potential Application of Peppermint (Mentha piperita L.), German Chamomile (Matricaria chamomilla L.) and Yarrow (Achillea millefolium L.) as Active Fillers in Natural Rubber Biocomposites, International Journal of Molecular Sciences 2021, Vol. 22, Page 7530 22 (2021) 7530. https://doi.org/10.3390/IJMS22147530.

[30] S. Narath, S.K. Koroth, S.S. Shankar, B. George, V. Mutta, S. Wacławek, M. Čern\'\ik, V.V.T. Padil, R.S. Varma, Cinnamomum tamala leaf extract stabilized zinc oxide nanoparticles: A promising photocatalyst for methylene blue degradation, Nanomaterials 11 (2021) 1558.

[31] P.K. Jain, A. Soni, P. Jain, J. Bhawsar, Phytochemical analysis of Mentha spicata plant extract using UV-VIS, FTIR and GC/MS technique, J Chem Pharm Res 8 (2016) 1–6.

[32] T. Carballo, M.V. Gil, X. Gómez, F. González-Andrés, A. Morán, Characterization of different compost extracts using Fourier-transform infrared spectroscopy (FTIR) and thermal analysis, Biodegradation 19 (2008) 815–830.

[33] A.K. Mittal, Y. Chisti, U.C. Banerjee, Synthesis of metallic nanoparticles using plant extracts, Biotechnol Adv 31 (2013) 346–356. https://doi.org/10.1016/J.BIOTECHADV.2013.01.003.

[34] V.K. Sharma, R.A. Yngard, Y. Lin, Silver nanoparticles: Green synthesis and their antimicrobial activities, Adv Colloid Interface Sci 145 (2009) 83–96. https://doi.org/10.1016/J.CIS.2008.09.002.

[35] S.M. Pourmortazavi, M. Taghdiri, V. Makari, M. Rahimi-Nasrabadi, H. Batooli, Reducing power of Eucalyptus oleosa leaf extracts and green synthesis of gold nanoparticles using the extract, Int J Food Prop 20 (2017) 1097–1103. https://doi.org/10.1080/10942912.2016.1203334.

[36] S. ALBAYRAK, O. SA\uGDIÇ, A. AKSOY, Bitkisel ürünlerin ve g{\i}dalar{\i}n antioksidan kapasitelerinin belirlenmesinde kullan{\i}lan yöntemler, Erciyes Üniversitesi Fen Bilimleri Enstitüsü Fen Bilimleri Dergisi 26 (2010) 401–409.

[37] P.G. Krishna, P. Chandra Mishra, M.M. Naika, M. Gadewar, P.P. Ananthaswamy, S. Rao, S.R. Boselin Prabhu, K.V. Yatish, H.G. Nagendra, M. Moustafa, others, Photocatalytic activity induced by metal nanoparticles synthesized by sustainable approaches: A comprehensive review, Front Chem 10 (2022) 917831.

[38] G.A. Valencia, L.C.O. De Vercik, L.G. Ferreira, J.H.R. Llanos, A. Vercik, Synthesis and characterisation of gold nanoparticles using Mentha piperita leaf extract: A green, non-toxic and rapid method, International Journal of Nano and Biomaterials 5 (2014) 181–192. https://doi.org/10.1504/IJNBM.2014.066905.

[39] M.S. Mohammad, P. Shyam, Structural Analysis of Biogenic Copper Oxide Nanoparticles, and their Bio-Activity Assessment, Bionanoscience 13 (2023) 2265–2275. https://doi.org/10.1007/S12668-023-01168-0/FIGURES/7.

[40] S. Ayadi Hassan, P. Ghadam, A. Abdi Ali, One step green synthesis of Cu nanoparticles by the aqueous extract of Juglans regia green husk: assessing its physicochemical, environmental and biological activities, Bioprocess Biosyst Eng 45 (2022) 605–618. https://doi.org/10.1007/S00449-022-02691-2/FIGURES/11.

[41] A.M. Pourrahimi, D. Liu, L.K.H. Pallon, R.L. Andersson, A. Martínez, M. Abad, J.-M. Lagarón, L. Lagarón, M.S. Hedenqvist, V. Ström, S. Ström, U.W. Gedde, R.T. Olsson, Water-based synthesis and cleaning methods for high purity ZnO nanoparticles-comparing acetate, chloride, sulphate and nitrate zinc salt precursors †, (2014). https://doi.org/10.1039/c4ra06651k.

[42] M.S. Yedurkar, D.K. Punjabi, B.C. Maurya, A.P. Mahanwar, Biosynthesis of zinc oxide nanoparticles using Euphorbia milii leaf extract-A green approach, Mater Today Proc 5 (2018) 22561–22569.

[43] Z. Hasnain, S. Zafar, U. Shafqat, S. Perveen, N. Iqbal, S.A. Qaisrani, M.B. Chattha, S. Mumtaz, Antibacterial activity of eco-friendly zinc nanoparticles prepared from leaf extract of Mentha piperita L, Pak J Pharm Sci 33 (2020) 2413–2416.

[44] M.M. Modena, B. Rühle, T.P. Burg, S. Wuttke, Nanoparticle characterization: what to measure?, Advanced Materials 31 (2019) 1901556.

[45] C.R. Mendes, G. Dilarri, C.F. Forsan, V. de M.R. Sapata, P.R.M. Lopes, P.B. de Moraes, R.N. Montagnolli, H. Ferreira, E.D. Bidoia, Antibacterial action and target mechanisms of zinc oxide nanoparticles against bacterial pathogens, Scientific Reports 2022 12:1 12 (2022) 1–10. https://doi.org/10.1038/s41598-022-06657-y.

[46] S.H. Bae, J. Yu, T.G. Lee, S.J. Choi, Protein Food Matrix–ZnO Nanoparticle Interactions Affect Protein Conformation, but May not Be Biological Responses, International Journal of Molecular Sciences 2018, Vol. 19, Page 3926 19 (2018) 3926. https://doi.org/10.3390/IJMS19123926.

[47] J. Miao, Z. Jia, H.B. Lu, D. Habibi, L.C. Zhang, Heterogeneous photocatalytic degradation of mordant black 11 with ZnO nanoparticles under UV–Vis light, J Taiwan Inst Chem Eng 45 (2014) 1636–1641. https://doi.org/10.1016/J.JTICE.2013.11.007.

[48] H. Yang, J. Zhang, Z. Li, J. Huang, J. Wu, Y. Zhang, H. Ge, Y. Zhao, Antibacterial Effect of Low-Concentration ZnO Nanoparticles on Sulfate-Reducing Bacteria under Visible Light, Nanomaterials 2023, Vol. 13, Page 2033 13 (2023) 2033. https://doi.org/10.3390/NANO13142033.

[49] Product File ZnO Sigma Aldrich, (n.d.). https://www.sigmaaldrich.com/specification-sheets/154/134/544906-BULK_____ALDRICH__.pdf (accessed September 3, 2023).

[50] P. Hemnil, Y. Prapawasit, V. Karthikeyan, T. Wongwuttanasatian, V. Seithtanabutara, Novel cubic heterojunction Fe2O3/ZnO composite for the photocatalyst application, Mater Today Proc 75 (2023) 1–8. https://doi.org/10.1016/J.MATPR.2022.10.010.

[51] View of Synthesis of ZnO nanostructures and its effect on linear-nonlinear optical properties, (n.d.). https://etnano.com/index.php/en/article/view/233/217 (accessed February 12, 2024).

[52] D. Maity, A.S. Sabnis, Anhydride-cured epoxidized dehydrated castor oil (EDCO) containing organically modified zinc oxide (ZnO) nanoparticles, Journal of Industrial and Engineering Chemistry 123 (2023) 459–475. https://doi.org/10.1016/J.JIEC.2023.03.064.

[53] W. Chen, X. Liu, Y. Liu, H. Il Kim, Synthesis of microcapsules with polystyrene/ZnO hybrid shell by Pickering emulsion polymerization, Colloid Polym Sci 288 (2010) 1393–1399. https://doi.org/10.1007/S00396-010-2277-8/FIGURES/7.

[54] L. A. Avinash Chunduri, A. Kurdekar, B. Eswarappa Pradeep, M. Kumar Haleyurgirisetty, V. K, I. K. Hewlett, Streptavidin conjugated ZnO nanoparticles for early detection of HIV infection, Adv Mater Lett 8 (2017) 472–480. https://doi.org/10.5185/AMLETT.2017.6579.

[55] M.A. Abomuti, E.Y. Danish, A. Firoz, N. Hasan, M.A. Malik, Green synthesis of zinc oxide nanoparticles using salvia officinalis leaf extract and their photocatalytic and antifungal activities, Biology (Basel) 10 (2021) 1075.

[56] T. Dayakar., K. Venkateswara Rao., K. Bikshalu., V. Rajendar., S.H. Park, Novel synthesis and structural analysis of zinc oxide nanoparticles for the non enzymatic glucose biosensor, Materials Science and Engineering: C 75 (2017) 1472–1479. https://doi.org/10.1016/J.MSEC.2017.02.032.

[57] P. Jamdagni, P. Khatri, J.S. Rana, Green synthesis of zinc oxide nanoparticles using flower extract of Nyctanthes arbor-tristis and their antifungal activity, J King Saud Univ Sci 30 (2018) 168–175. https://doi.org/10.1016/J.JKSUS.2016.10.002.

[58] H. Babu Boppudi, Y. Subba Rao, C. Kuchi, A. Ramesh Babu, V. Govinda, M. Jagadeesh, M. Lavanya, Zinc oxide nanoparticles as an efficient antioxidant, photocatalyst, and heterogeneous catalyst in C–P bond synthesis, Results Chem 6 (2023) 101227. https://doi.org/10.1016/J.RECHEM.2023.101227.

[59] A. Muthuvel, M. Jothibas, C. Manoharan, Effect of chemically synthesis compared to biosynthesized ZnO-NPs using Solanum nigrum leaf extract and their photocatalytic, antibacterial and in-vitro antioxidant activity, J Environ Chem Eng 8 (2020) 103705. https://doi.org/10.1016/J.JECE.2020.103705.

[60] W.R. Rolim, M.T. Pelegrino, B. de Araújo Lima, L.S. Ferraz, F.N. Costa, J.S. Bernardes, T. Rodigues, M. Brocchi, A.B. Seabra, Green tea extract mediated biogenic synthesis of silver nanoparticles: Characterization, cytotoxicity evaluation and antibacterial activity, Appl Surf Sci 463 (2019). https://doi.org/10.1016/j.apsusc.2018.08.203.

[61] P. Shubha, M.L. Gowda, K. Namratha, H.B. Manjunatha, K. Byrappa, In vitro and In vivo evaluation of green-hydrothermal synthesized ZnO nanoparticles, J Drug Deliv Sci Technol 49 (2019) 692–699. https://doi.org/10.1016/J.JDDST.2018.12.017.

[62] M. Rajapriya, S.A. Sharmili, R. Baskar, R. Balaji, N.S. Alharbi, S. Kadaikunnan, J.M. Khaled, K.F. Alanzi, B. Vaseeharan, Synthesis and Characterization of Zinc Oxide Nanoparticles Using Cynara scolymus Leaves: Enhanced Hemolytic, Antimicrobial, Antiproliferative, and Photocatalytic Activity, J Clust Sci 31 (2020) 791–801. https://doi.org/10.1007/S10876-019-01686-6/FIGURES/9.

[63] S.S. Sana, R. Vadde, R. Kumar, S.K. Arla, A.R. Somala, K.S.V. Krishna Rao, Z. Zhijun, V.K.N. Boya, K. Mondal, N. Mamidi, Eco-friendly and facile production of antibacterial zinc oxide nanoparticles from Grewia flavescens (G. flavescens) leaf extract for biomedical applications, J Drug Deliv Sci Technol 80 (2023) 104186. https://doi.org/10.1016/J.JDDST.2023.104186.

[64] C. Corbo, R. Molinaro, A. Parodi, N.E. Toledano Furman, F. Salvatore, E. Tasciotti, The impact of nanoparticle protein corona on cytotoxicity, immunotoxicity and target drug delivery, Nanomedicine 11 (2016) 81–100. https://doi.org/10.2217/NNM.15.188.

[65] G. Bashiri, M.S. Padilla, K.L. Swingle, S.J. Shepherd, M.J. Mitchell, K. Wang, Nanoparticle protein corona: from structure and function to therapeutic targeting, Lab Chip 23 (2023) 1432–1466. https://doi.org/10.1039/D2LC00799A.

[66] R.E. Wang, L. Tian, Y.H. Chang, A homogeneous fluorescent sensor for human serum albumin, J Pharm Biomed Anal 63 (2012) 165–169. https://doi.org/10.1016/J.JPBA.2011.12.035.

[67] N.J. White, E. Gonzalez, E.E. Moore, H.B. Moore, Fibrinogen, Trauma Induced Coagulopathy (2023) 101–116. https://doi.org/10.1007/978-3-030-53606-0_8.

[68] K. Stang, S. Krajewski, B. Neumann, J. Kurz, M. Post, S. Stoppelkamp, S. Fennrich, M. Avci-Adali, D. Armbruster, C. Schlensak, I.A. Burgener, H.P. Wendel, T. Walker, Hemocompatibility testing according to ISO 10993-4: Discrimination between pyrogen- and device-induced hemostatic activation, Materials Science and Engineering: C 42 (2014) 422–428. https://doi.org/10.1016/J.MSEC.2014.05.070.

[69] A.J. Stewart, C.A. Blindauer, S. Berezenko, D. Sleep, P.J. Sadler, Interdomain zinc site on human albumin, Proc Natl Acad Sci U S A 100 (2003) 3701–3706. https://doi.org/10.1073/PNAS.0436576100/SUPPL_FILE/6576FIG7.PDF.

[70] E.P. Babu, A. Subastri, A. Suyavaran, K. Premkumar, V. Sujatha, B. Aristatile, G.M. Alshammari, V. Dharuman, C. Thirunavukkarasu, Size Dependent Uptake and Hemolytic Effect of Zinc Oxide Nanoparticles on Erythrocytes and Biomedical Potential of ZnO-Ferulic acid Conjugates, Scientific Reports 2017 7:1 7 (2017) 1–12. https://doi.org/10.1038/s41598-017-04440-y.

[71] M. Mitjans, L. Marics, M. Bilbao, A.S. Maddaleno, J.J. Piñero, M.P. Vinardell, Size Matters? A Comprehensive In Vitro Study of the Impact of Particle Size on the Toxicity of ZnO, Nanomaterials 13 (2023) 1800. https://doi.org/10.3390/NANO13111800/S1.

[72] E. Dinga, D.M.N. Mthiyane, U. Marume, T.L. Botha, S. Horn, R. Pieters, V. Wepener, A. Ekennia, D.C. Onwudiwe, Biosynthesis of ZnO nanoparticles using Melia azedarach seed extract: Evaluation of the cytotoxic and antimicrobial potency, OpenNano 8 (2022) 100068. https://doi.org/10.1016/J.ONANO.2022.100068.

[73] E.F. El-Belely, M.M.S. Farag, H.A. Said, A.S. Amin, E. Azab, A.A. Gobouri, A. Fouda, Green Synthesis of Zinc Oxide Nanoparticles (ZnO-NPs) Using Arthrospira platensis (Class: Cyanophyceae) and Evaluation of their Biomedical Activities, Nanomaterials 2021, Vol. 11, Page 95 11 (2021) 95. https://doi.org/10.3390/NANO11010095.

[74] H. Maheswaran, S. Djearamane, A.C. Tanislaus Antony Dhanapal, L.S. Wong, Cytotoxicity of green synthesized zinc oxide nanoparticles using Musa acuminata on Vero cells, Heliyon 10 (2024) e31316. https://doi.org/10.1016/J.HELIYON.2024.E31316/ASSET/C2C37602-2DEA-4667-82F9-5C2A9065C484/MAIN.ASSETS/GR8.JPG.

[75] A.S. Shaban, M.E. Owda, M.M. Basuoni, M.A. Mousa, A.A. Radwan, A.K. Saleh, Punica granatum peel extract mediated green synthesis of zinc oxide nanoparticles: structure and evaluation of their biological applications, Biomass Convers Biorefin 14 (2024) 12265–12281. https://doi.org/10.1007/S13399-022-03185-7/FIGURES/10.

a.